

Article

Phase-Shifting Adaptive LLC Resonant Converter with Reduced Turn-Off Loss in Wide Voltage Application

Hongxun Jiang¹ and Xiumei Yue^{2,*}

¹ Sichuan Electromechanical Institute of Vocation and Technology, Panzhihua 617000, China; pzh_jhx@163.com

² College of Electrical and Information Engineering, Hunan University, Changsha 410082, China

* Correspondence: yuexm@hnu.edu.cn

Abstract: In this paper, a hybrid control method with adaptive phase-shifting modulation (PSM) and pulse-frequency modulation (PFM) is proposed to optimize the steady-state performance of an LLC resonant converter in wide voltage-gain range application. For the primary-side switches under the hybrid control method, zero-voltage switching (ZVS) performance is maintained over wide voltage-gain range and the turn-off loss is reduced; therefore, the converter reconciles wide voltage-gain range and high efficiency. Mode characteristics under different phase-shifting-angle- θ and switching-frequency- f_s combinations is analyzed, and then the soft-switching characteristic is revealed. By introducing time domain analysis, the turn-on current of the primary-side switches is calculated, and thus the ZVS boundary of different θ and f_s combinations is inferred. In addition, to acquire the optimum steady-state operation of the converter, the turn-off current is calculated; by making the converter work near to the minimum turn-off current operating point, the turn-off loss can be reduced greatly. With the principles of achieving ZVS performance and minimizing turn-off current, the phase-shifting angle θ of PSM is designed to be adaptive to the reference output voltage, no additional circuits are needed, and the two control degrees (θ and f_s) are simplified to one (f_s). The simulation and experiment are developed to verify the feasibility and effectiveness of the hybrid control method; the results show that ZVS performance is maintained at wide voltage-gain range and the turn-off current of the hybrid control method is reduced to that of the single PFM, and thus the turn-off loss is reduced. The efficiency comparison validates the fact that the hybrid control method has less power loss than single PSM and single PFM.



Citation: Jiang, H.; Yue, X. Phase-Shifting Adaptive LLC Resonant Converter with Reduced Turn-Off Loss in Wide Voltage Application. *Energies* **2024**, *17*, 1555. <https://doi.org/10.3390/en17071555>

Academic Editor: Javier Contreras

Received: 28 January 2024

Revised: 10 March 2024

Accepted: 11 March 2024

Published: 25 March 2024



Copyright: © 2024 by the authors. Licensee MDPI, Basel, Switzerland. This article is an open access article distributed under the terms and conditions of the Creative Commons Attribution (CC BY) license (<https://creativecommons.org/licenses/by/4.0/>).

Keywords: LLC resonant converter; wide voltage gain; hybrid control; soft-switching performance; turn-off loss

1. Introduction

The LLC resonant converter is one of the most promising converters in isolated DC-DC applications, such as flat-panel TVs, laptop adapters, servers and so on, because of its attractive features: smooth waveforms, soft-switching characteristic for both primary-side MOSFET and secondary-side diodes [1–6], high efficiency at wide load range and high power density. The resonant network of the LLC resonant converter is composed of three passive devices, so there are two resonant frequency points. Other resonant converters, such as LCC [5–7] and LCLC [8–10] are also used in various industry applications for these similar features.

For LLC resonant converters, one of the most prevalent modulation strategies is pulse-frequency modulation (PFM); by regulating the switching frequency, the impedance of the resonant rank can be adjusted, and as a result, the output voltage is regulated. However, when it comes to the application where the input voltage or output voltage is wide such as electric car charging pile and solar energy applications, the switching frequency will swing within a wide range to meet the voltage-gain requirement, which brings challenges to the magnetic components, gate drivers and EMI performance. In addition, wide voltage gain

usually means small inductance ratio, which result in a large reactive power circulation. Therefore, it is very difficult to optimally design the LLC converter adapted to wide voltage gain with traditional topology and the single-PFM control method. To widen the voltage gain for the LLC resonant converter, many articles in the literature develop improvements from the topology reconfiguration and multi-degree modulation strategies.

The reconfiguration of the resonant tank has attracted much attention for widening the voltage-gain range, including the resonant inductor L_r , resonant capacitor C_r , magnetic inductor L_m and transformer turns ratios n . The modification focuses on variable L_m , including adding auxiliary LC structures [11,12] and auxiliary transformer winds [13]. Moreover, the resonant capacitor C_r can be replaced by a switch-controlled capacitor (SCC); the equivalent resonant capacitance is adjusted by high-frequency switching to meet different voltage-gain demand [14,15]. These methods all need additional circuits, which increases the cost the converter and reduces the power density of the converter. Other topology reconfiguration methods are also proposed: paper [16] transits the half-bridge and full-bridge mode in the primary side of the full-bridge LLC converter, and wide voltage gain can be achieved. Paper [17] proposes an interleaved secondary-side modulated LLC resonant converter to achieve wide output range. Paper [18] forms a different inverter-bridge type with six MOSFETs, but only steady states are considered and the cost of the inverter bridge is high. These methods all suffer from the smooth-switching problem, dynamically. Paper [19] proposes a novel topology with an additional PWM switch at the secondary side for narrowing down the frequency range. Paper [20] uses a magnetic amplifier auxiliary post regulator to extend voltage gain, while switching frequency f_s keeps it at a constant value, but the control is complex and the cost is high. A multi-mode hybrid LLC resonant converter with wide output voltage range is proposed in [21]. In the absence of an auxiliary switch, the converter can operate in three different modes by controlling the drive signal of the main switch. A novel LLC converter with single input and double output for wide output voltage applications is proposed in [22]. The H5 bridge is used on the main side and is connected to two separate resonant networks.

The topology reconfiguration methods all require an extra passive or active device, and the cost and control complexity may reduce the benefits of the LLC resonant converter. As a result, the hybrid modulation method as a supplement of PFM is being widely researched. Phase-shifting modulation (PSM) is a promising supplement to the PFM in the LLC resonant converter, and the steady-state analysis of PSM in the LLC converter is studied in [23]. In [24,25], by controlling the phase-shifting angle, the equivalent duty cycle can be adjusted so as to regulate the output, but when the phase-shifting angle is large it may suffer from hard switching to the lagging bridge. Paper [26] applies an FM/PSM mode switching to support a wider voltage gain, but the ZVS constraint is not quantified. Paper [27] introduces a load-adaptive phase-shifting control for a light load of the LLC converter, but the design method only aims at improving the efficiency at light load, and the wide voltage gain and heavy load efficiency is not optimized. Paper [28] proposes a frequency adaptive phase-shifting modulation control for wide input voltage applications; the phase-shifting control scheme is applied in the secondary side, and thus synchronous rectification and its control circuit is needed, which is not cost-effective. Pulse width modulation (PWM) for the LLC converter is also proposed in [29,30] for the primary side and secondary side to regulate the output voltage, but the extra circuit will result in high cost. In [31,32], the burst mode (BM) strategy is employed in light and no-load conditions to achieve a wide output range, but a high-frequency oscillation exists during the OFF state and will result in EMI problems. In [33], a simplified optimal trajectory control based on the adaptive burping mode for the high-frequency LLC converter is proposed and implemented by a low-cost single-chip microcomputer. A new hybrid control method is proposed in [34]. The strategy combines burp mode control and phase shift control of the LLC converter. Burp mode control can adjust the output voltage from zero to the maximum, and phase shift control can reduce the increased resonant current during burping. In order to solve the problem of LLC light-load control, a new LLC resonant converter modulation method is proposed in

Reference [35], which simplifies the control design and maintains high efficiency over the entire load range.

To widen the voltage-gain range and keep the low cost and high efficiency of the LLC converter, a hybrid control method with adaptive PSM and PFM is proposed to optimize the steady-state performance of the LLC resonant converter in a wide voltage-gain range application. For the primary-side switches under the hybrid control, zero-voltage switching (ZVS) performance is maintained over wide voltage range and the turn-off loss is reduced; therefore, the converter reconciles wide voltage-gain range and high efficiency. Mode characteristics under different phase-shifting-angle- θ and switching-frequency- f_s combinations are analyzed, and then the soft-switching characteristic is revealed. By introducing time domain analysis, the turn-on current of the primary-side switches is calculated, and thus the ZVS boundary of different θ and f_s combinations is inferred. In addition, to acquire the optimum steady-state operation of the converter, the turn-off current is calculated; by making the converter work near to the minimum turn-off current operating point, the turn-off loss can be greatly reduced. With the principles of achieving ZVS performance and minimizing turn-off current, the phase-shifting angle θ of PSM is designed to be adaptive to the reference output voltage; no additional circuits are needed and the two control degrees (θ and f_s) are simplified to one (f_s). The simulation and a 1 kW/output voltage 200–500 V experiment prototype are built to validate the feasibility and effectiveness of the proposed hybrid control method. Both results show the hybrid control method can maintain ZVS performance at wide output voltage range and wide load range when compared to single PSM; the sum of the turn-off currents of the primary-side leading- and lagging-bridge switches is reduced when compared to the single PFM, and thus turn-off loss is reduced. The efficiency comparison validates the fact that the hybrid control method has less power loss than single PSM and single PFM.

This paper is organized as follows: Section 2 introduces the working principles when applying hybrid PSM and PFM, and then the soft-switching performance characteristic of different working modes is clarified. Section 3 designs an adaptive PSM control method with PFM to regulate the output voltage based on time domain analysis. Sections 4 and 5 provide PSIM simulation and experiment results of the proposed control methods, single PSM and single PFM. Finally, this paper is concluded in Section 6.

2. Working Principles of LLC Converter with Phase-Shifting and Frequency Modulation

In this section, the working principles of the LLC resonant converter when applying hybrid PSM and PFM are discussed, and the soft-switching performance characteristic is inferred. Part A introduces several definitions of the terms relating to the LLC resonant converter and its fundamental harmonic approximation (FHA) analysis results. Part B shows four main operation modes and their soft-switching performance characteristic.

2.1. Definition and FHA Analysis of LLC Resonant Converter

The LLC resonant converter is shown in Figure 1. It is mainly composed of a DC input V_{in} , an input filtering capacitor C_{in} , a full-bridge inverter, a resonant tank, a high-frequency transformer T_1 , a full-bridge rectifier, a large output-filter capacitor C_{out} and load R_o . The full-bridge inverter consists of four power switches Q_1 – Q_4 , and D_1 – D_4 and C_1 – C_4 are the parasitic diode and capacitor of the power switches, separately. The resonant tank consists of resonant inductor L_r , resonant capacitor C_r and magnetic inductor L_m . V_{AB} is the output voltage of the inverter bridge, i_{Lr} is the resonant current, v_{C_r} is the voltage on C_r , i_m is the magnetizing current of L_m , i_{rect} is the rectified current, which is composed of the difference between i_{Lr} and i_m , i_o is the load current, V_o is the DC output voltage, and f_r is the resonant frequency which is defined in (1).

$$f_r = \frac{1}{2\pi\sqrt{L_r C_r}} \quad (1)$$

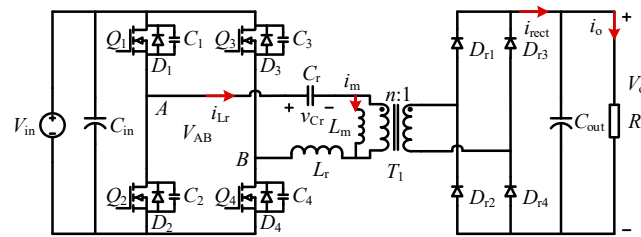


Figure 1. LLC resonant converter topology.

Q_1 – Q_4 are all turned on with a 50% duty cycle, and Q_1 is complementary to Q_2 , while Q_3 is complementary to Q_4 . By adjusting the switching frequency, the impedance of the resonant tank is changed, and the output is regulated by PFM. By shifting the switching angle θ between Q_1 and Q_4 , V_{AB} is adjusted to a three-level square wave with a different proportion of zero-voltage level, and then output is regulated by PSM. When $\theta = 0^\circ$, V_{AB} is a two-level square wave without a zero-voltage level; when $\theta = 180^\circ$, V_{AB} equals 0, and the output voltage can be regulated to 0, theoretically.

Figure 2 shows the typical gain characteristic of the LLC resonant converter based on FHA when applying PFM. The working zone can be simply divided into three types: #1 is the boost zone, where the switching frequency f_s is less than the resonant frequency f_r , and the voltage gain is larger than 1. The converter can realize primary-side ZVS and secondary-side ZCS when working at #1. However, reactive power circulation would reduce the benefit when the voltage-gain range is wide at this zone. The buck zone is #2: when the switching frequency f_s is larger than the resonant frequency f_r , and the voltage gain is less than 1, the converter realizes primary-side ZVS but loses secondary-side ZCS when working in this area. The capacitive zone is #3: the whole resonant tank has a capacitive load, ZVS performance is lost, and it is necessary to avoid working in this area for MOSFET.

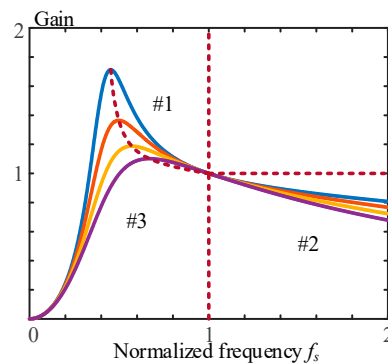


Figure 2. Gain characteristic based on FHA under different Q_s .

Both #1 and #2 have advantages for realizing ZVS performance: #1 can fully meet the demand for narrow voltage-gain range application, but when it comes to wide gain range, only #1 participation will result in a large reactive power circulation, which undermines the benefits of the converter. To solve this, #2 also participates in the work to regulate the gain, but the frequency range will be large when the voltage range and load range are wide, which is not good for the design of magnetic components and the gate driver. PSM in #2 can change the equivalent input of the resonant tank to reduce voltage gain with a narrow frequency range, but ZVS performance will be hard to achieve if the phase-shifting angle θ is large. To solve these problems, in this paper, an adaptive phase-shifting angle is proposed to ensure the ZVS performance in #2 and reduce the sum of the turn-off currents; the design principle will be discussed in Section 3.

2.2. Key Working Waveforms When Applying PSM

In this part, the working zone #2 is mainly been discussed where the working frequency f_s is larger than the resonant frequency f_r . The equivalent circuit of the converter is shown in Figure 3: a , S_0 and b are state parameters which consist of different modes, and Table 1 shows the A–I stage with different state combinations.

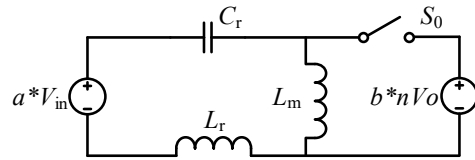


Figure 3. Equivalent circuit with PSM.

Table 1. Different stage under different state combinations.

a		+1			0			-1	
S_0	on	off	on	on	off	on	on	off	on
b	-1	\	+1	+1	\	-1	-1	\	+1
stage	A	B	C	D	E	F	G	H	I

One complete switching period of the LLC converter is composed of stage A–I, as paper [21] reveals: the stage combinations ACD, CDE, CDF and CDEF are the most common modes, while other modes only occur at very light load, which is not discussed in this paper. The four types of working modes correspond to different phase-shifting-angle- θ and switching-frequency- f_s combinations at #2 working zone. Type 1 represents the situation when f_s is large and θ is small. In this type, the converter performs like a single PFM; the primary-side ZVS can be guaranteed, and the secondary-side ZCS is lost. This type can be divided into five working modes at a positive half cycle, as Figure 4 shows. When including the dead time, the negative half cycle is similar to the positive, which will not be explained repeatedly.

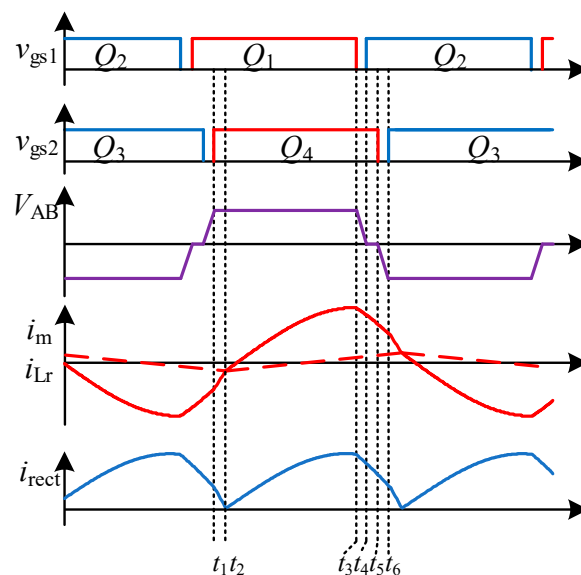


Figure 4. Key waveforms of type 1 ACD.

Mode 1 [t_1 – t_2]: In this mode, the inverter-bridge output voltage V_{AB} equals V_{in} , L_m is clamped by $-nV_o$, i_m decreases linearly, L_r resonates with C_r , i_{Lr} rises rapidly, and the secondary-side rectifier diodes D_{r2} and D_{r3} conduct to transfer energy to the load side.

Mode 2 [t_2 – t_3]: At t_2 , i_m drops to the same value as i_{Lr} , while V_{AB} still equals V_{in} , but the resonant process will result in a difference in current between i_{Lr} and i_m . Then D_{r1} and D_{r4} are turned on and D_{r2} and D_{r3} are turned off. Due to the continuous conduction mode of the diodes, D_{r2} and D_{r3} lose ZCS performance. L_m begins to be clamped by nV_o and rises linearly, and L_r continues to resonate with C_r .

Mode 3 [t_3 – t_4]: This is the dead-time mode. After Q_1 turns off, i_{Lr} is positive, then C_2 is discharged and C_1 is charged until the D_2 freewheels. Thus, this mode provides the conditions for the ZVS performance of Q_2 .

Mode 4 [t_4 – t_5]: After Q_2 turns on, V_{AB} equals 0, L_r and C_r are still resonating, L_m is clamped by nV_o , i_m rises linearly, and D_{r1} and D_{r4} conduct to transfer energy to the load side.

Mode 5 [t_5 – t_6]: This is the dead-time mode. After Q_4 turns off, i_{Lr} is positive, then C_3 is discharged and C_4 is charged until the D_2 freewheels. Thus, this mode provides the conditions for the ZVS of Q_3 . Compared to mode 3, at this mode, due to i_{Lr} decreasing rapidly at mode 4, the turn-off current of Q_4 is reduced, and thus the turn-off loss is reduced. Owing to the reduction in i_{Lr} , the ZVS implementation for Q_3 will be harsher, so a minimum value of i_{Lr} needs to be maintained for a reliable ZVS performance of Q_3 .

Type 2 represents the situation when f_s and θ are moderate, and the load is light. In this type, L_m will join to the resonance between L_r and C_r at 0 voltage level of V_{AB} , so the secondary-side ZCS is obtained. This type can be divided into five working modes at the positive half cycle, as Figure 5 shows, when including the dead time. Due to the limited space of the article, only Mode 4 [t_4 – t_5] is discussed. Other modes are similar to the working condition of the ACD type.

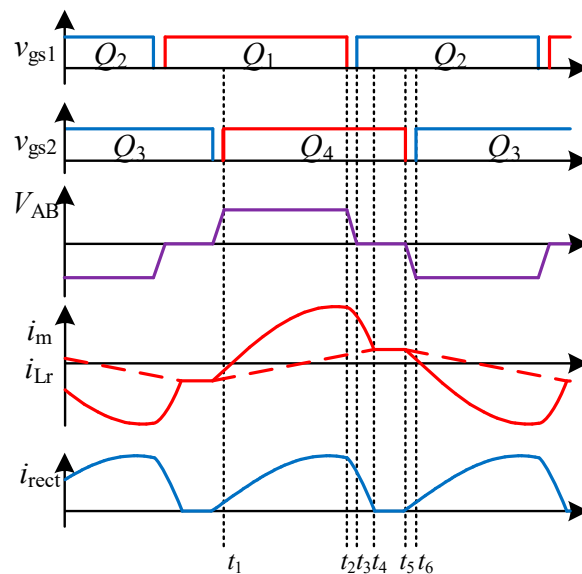


Figure 5. Key waveforms of type CDE.

Mode 4 [t_4 – t_5]: At t_4 , i_{Lr} drops to the same value as i_m , then L_m begins to join to the resonance between L_r and C_r ; i_m keeps consistent with i_{Lr} , and thus no current transits to the secondary side, and D_{r1} and D_{r4} achieve ZCS performance. Due to the i_{Lr} drops in mode 3 [t_4 – t_5], the turn-off loss of Q_4 is reduced and the ZVS implementation for Q_3 will be harsher. A minimum value of i_{Lr} needs to be maintained for a reliable ZVS performance of Q_3 .

Type 3 represents the situation when f_s is low but θ is large and the load is heavy. Due to this reason, the ZVS performance of the lagging bridge is easily lost, and the hard switching performance will impact the reliability and efficiency seriously. This type can also be divided into five working modes at a positive half cycle as Figure 6 shows, when

including the dead time. Due to the limited space of the article, only mode 4 $[t_4-t_5]$ and mode 5 $[t_5-t_6]$ are discussed; other modes are similar to the CDE type.

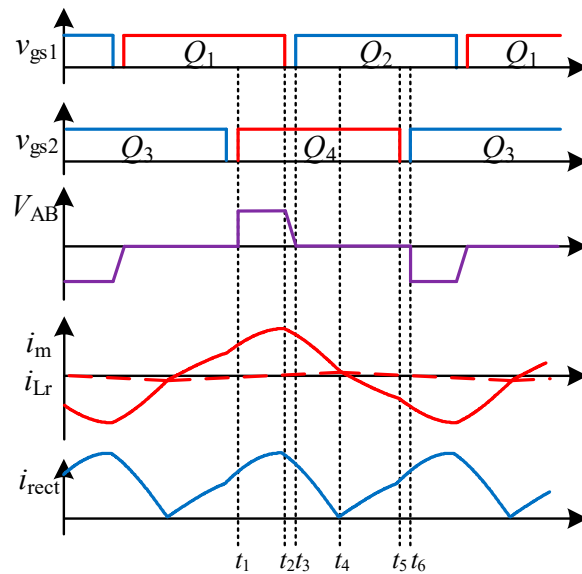


Figure 6. Key waveforms of type CDF.

Mode 4 $[t_4-t_5]$: Due to C_r being charged by a large current i_{Lr} in $[t_1-t_4]$, when i_{Lr} drops to the same value as i_m at t_4 , L_m will not join in with the resonance with L_r and C_r , and the different current between i_{Lr} and i_m will make D_{r1} and D_{r4} turn off and D_{r2} and D_{r3} turn on. This means D_{r1} and D_{r4} lose ZCS performance. In this mode, i_{Lr} keeps decreasing and then changes to the negative direction, which will make Q_3 lose ZVS performance.

Mode 5 $[t_5-t_6]$: This is the dead-time mode. After Q_4 turns off, owing to the negative i_{Lr} , D_4 freewheels, so the energy stored in C_3 will not be released, and the ZVS performance of Q_3 is lost.

Type 4 represents the situation which falls between type 3 and type 4. It can be divided into six working modes at a positive half cycle, as Figure 7 shows, when including the dead time. Mode 4 $[t_4-t_5]$ is equal to mode 4 in type 2, and mode 5 $[t_5-t_6]$ is equal to mode 5 in type 3. Thus, it can be inferred that the ZVS performance of Q_3 is hard to achieve, and the ZCS performance of the rectifier diodes is lost.

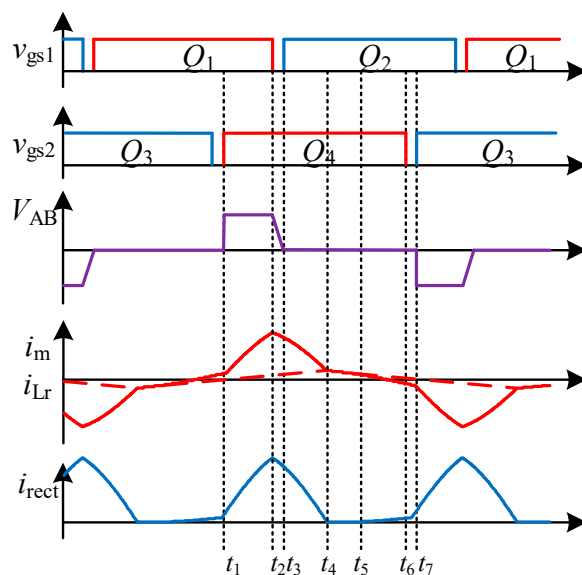


Figure 7. Key waveforms of type CDEF.

From the key waveform of the four different types, the soft-switching performance characteristic can be concluded as in Table 2. It can be seen that only the ACD type and the CDE type have the ZVS characteristic for the primary-side switches, and that the ZCS characteristic for the secondary-side diodes only occurs at the CDE type. Thus, for the efficiency and reliability of the converter, only type ACD and type CDE are accepted, while type CDF and type CDEF should be avoided.

Table 2. Soft-switching performance under different working modes.

Working Mode	ACD	CDE	CDF	CDEF
Primary-Side ZVS	Achieved	Achieved	Lost	Hard to Achieve
Secondary-Side ZCS	Lost	Achieved	Lost	Lost

3. Design Principle of the Hybrid Control Method

As Section 2 reveals, ZVS performance only occurs at type ACD and type CDE. Traditional FHA analysis is hard to clarify and it is hard to distinguish the mode characteristic when applying hybrid PSM and PFM. In this section, time domain analysis is provided to calculate the turn-on current and turn-off current; thus, the ZVS boundary conditions can be figured out to determine the suitable hybrid PSM and PFM strategy. To reduce the turn-off loss of the primary-side switches, deducing the minimum turn-off current working point is another determination condition for the hybrid control strategy.

As the equivalent circuit shows in Figure 3, the time-domain equations of the A, C, D, E, and F stages can be list as (2)–(7). The equations include the state variables i_{Lr} , v_{Cr} and i_{Lm} . No matter what the stage is, the ampere–second balance equation of output-filter capacitor C_{out} can be listed as (8).

At stage A, V_{AB} equals V_{in} , L_r and C_r resonate, L_m is clamped by $-nV_o$, and i_m decreases linearly. The equation is shown as (2).

$$\begin{cases} i_{Lr}(t) = i_{Lr}(t_0) \cos \omega_r(t - t_0) \\ -[v_{Cr}(t_0) - V_{in} - nV_o] \sin \omega_r(t - t_0) / \sqrt{\frac{L_r}{C_r}} \\ v_{Cr}(t) = V_{in} + nV_o + [v_{Cr}(t_0) - V_{in} - nV_o] \cos \omega_r(t - t_0) \\ + \sqrt{\frac{L_r}{C_r}} i_{Lr}(t_0) \sin \omega_r(t - t_0) \\ i_m(t) = i_m(t_0) - \frac{nV_o}{L_m}(t - t_0) \end{cases} \quad (2)$$

where t_0 is the start time of the mode and ω_r is shown in (3).

$$\omega_r = 2\pi f_r \quad (3)$$

At stage C, V_{AB} equals V_{in} , L_r and C_r resonate, L_m is clamped by nV_o , and i_m increases linearly. The equation is shown as (4).

$$\begin{cases} i_{Lr}(t) = i_{Lr}(t_0) \cos \omega_r(t - t_0) \\ -[v_{Cr}(t_0) - V_{in} + nV_o] \sin \omega_r(t - t_0) / \sqrt{\frac{L_r}{C_r}} \\ v_{Cr}(t) = V_{in} - nV_o + [v_{Cr}(t_0) - V_{in} + nV_o] \cos \omega_r(t - t_0) \\ + \sqrt{\frac{L_r}{C_r}} i_{Lr}(t_0) \sin \omega_r(t - t_0) \\ i_m(t) = i_m(t_0) + \frac{nV_o}{L_m}(t - t_0) \end{cases} \quad (4)$$

At stage D, V_{AB} equals 0, L_r and C_r resonate, L_m is clamped by nV_o , and i_m increases linearly. The equation is shown as (5).

$$\begin{cases} i_{Lr}(t) = i_{Lr}(t_0) \cos \omega_r(t - t_0) \\ -[v_{Cr}(t_0) + nV_o] \sin \omega_r(t - t_0) / \sqrt{\frac{L_r}{C_r}} \\ v_{Cr}(t) = -nV_o + [v_{Cr}(t_0) + nV_o] \cos \omega_r(t - t_0) \\ + \sqrt{\frac{L_r}{C_r}} i_{Lr}(t_0) \sin \omega_r(t - t_0) \\ i_m(t) = i_m(t_0) + \frac{nV_o}{L_m}(t - t_0) \end{cases} \quad (5)$$

At stage E, V_{AB} equals 0. L_m joins in with the resonance between L_r and C_r , and L_m is no longer clamped by nV_o or $-nV_o$. The equation is shown as (6).

$$\begin{cases} i_{Lr}(t) = i_{Lr}(t_0) \cos \frac{1}{\sqrt{1+m}} \omega_r(t - t_0) \\ -\frac{1}{\sqrt{1+m}} v_{Cr}(t_0) \sin \frac{1}{\sqrt{1+m}} \omega_r(t - t_0) / \sqrt{\frac{L_r}{C_r}} \\ v_{Cr}(t) = v_{Cr}(t_0) \cos \frac{1}{\sqrt{1+m}} \omega_r(t - t_0) \\ + \sqrt{1+m} \sqrt{\frac{L_r}{C_r}} i_{Lr}(t_0) \sin \frac{1}{\sqrt{1+m}} \omega_r(t - t_0) \\ i_m(t) = i_{Lr}(t) \end{cases} \quad (6)$$

where m is the inductance ratio of L_m to L_r .

At stage F, V_{AB} equal to 0. L_r and C_r resonate, L_m is clamped by $-nV_o$, and i_m decreases linearly. The equation is shown as (7).

$$\begin{cases} i_{Lr}(t) = i_{Lr}(t_0) \cos \omega_r(t - t_0) \\ -[v_{Cr}(t_0) - nV_o] \sin \omega_r(t - t_0) / \sqrt{\frac{L_r}{C_r}} \\ v_{Cr}(t) = nV_o + [v_{Cr}(t_0) - nV_o] \cos \omega_r(t - t_0) \\ + \sqrt{\frac{L_r}{C_r}} i_{Lr}(t_0) \sin \omega_r(t - t_0) \\ i_m(t) = i_m(t_0) - \frac{nV_o}{L_m}(t - t_0) \end{cases} \quad (7)$$

$$\frac{1}{T_s} \int_0^{T_s} |i_{Lr}(t) - i_m(t)| dt = \frac{V_o}{nR_o} \quad (8)$$

By combing the resonance equation and the voltage gain, the turn-on current and turn-off current of the primary-side switches can be figured out under different phase-shifting-angle- θ and switching-frequency- f_s combinations, to design the optimum combination. The design principle is shown in Figure 8. At a specific V_{in} , V_o and P working condition, different θ and f_s values can be combined for the steady-state operation of the LLC converter. If the voltage gain is qualified for this working condition, then calculate the turn-on currents of the primary-side switches to estimate the ZVS performance; if the ZVS performance is obtained, then calculate the turn-off currents of the primary-side switches to acquire an optimum θ and f_s combination for minimum turn-off currents. Therefore, the hybrid control is determined based on the ZVS constraint and minimum turn-off currents.

The schematic of the control circuit is shown in Figure 9. The control system adopts a single-loop voltage control. The sampling output voltage V_o is compared with the output reference voltage V_{o_ref} to obtain the error value, and then the frequency f_s or duty cycle D is obtained by the PI controller. When the frequency f_s does not reach the peak or valley value, the output duty cycle D of the phase-shift control unit is only determined by the output reference voltage V_{o_ref} . When the load is light and the frequency reaches the peak value, if the output voltage is still higher than the reference value the phase-shift control unit will be triggered, making the phase-shift angle increase or decrease to D , so as to achieve regulation voltage output. However, when the load is light, the phase-shift angle is

large. Even if the converter is in the CDE combination mode, ZVS is easily lost, due to the small magnetizing current i_m .

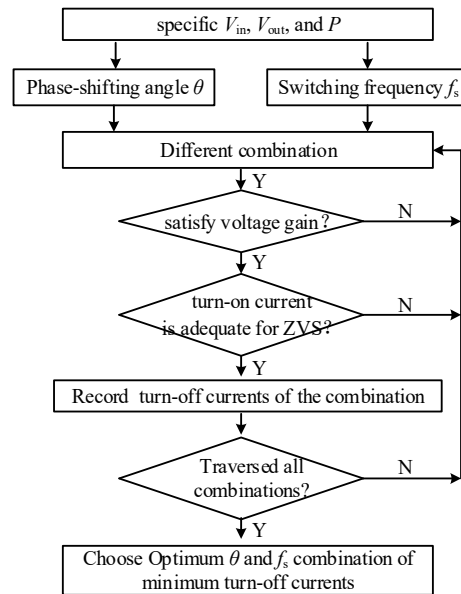


Figure 8. Hybrid control-strategy design principle.

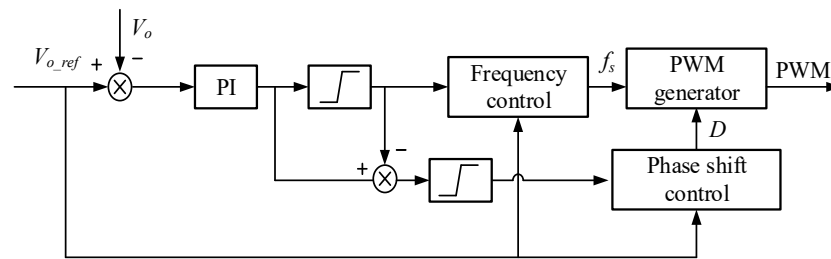


Figure 9. Schematic of control circuit.

Table 3 shows the parameters of an LLC converter, where the output voltage $V_o = 200\text{--}500\text{ V}$, the voltage-gain range is 2.5 times, and $V_o = 400\text{--}500\text{ V}$ is the boost mode of the LLC converter, while $V_o = 200\text{--}400\text{ V}$ is the buck mode. To explain the design principle of the hybrid control method, $V_o = 300\text{ V}$, $P = 200\text{ W}$, 400 W , 600 W , 800 W and 1 kW are presented for the hybrid control design.

Table 3. Value of Converter Parameters.

Parameter	Value
DC Input Voltage V_{in}	400 V
DC Output Voltage V_o	200–500 V
Resonant frequency f_r	150 kHz
Switching frequency f_s	90–300 kHz
Rated power P	1 kW
Resonant inductance L_r	94 μH
Resonant capacitance C_r	13.3 nF
Magnetic L_m	470 μH
Transformer ratio n	1:1

For the sake of description, define the function of phase-shifting angle θ and equivalent duty cycle D of V_{AB} as shown in Equation (9), and define normalized frequency f_n as shown in Equation (10).

$$D = 1 - \frac{\theta}{180^\circ} \quad 0^\circ \leq \theta \leq 180^\circ \quad (9)$$

$$f_n = \frac{f_s}{f_r} \tag{10}$$

Figure 10a shows different f_n and duty-cycle- D combinations at $V_o = 300$ V under different loads, and it can be concluded that there are innumerable combinations at a certain voltage gain and load. Figure 10b shows the turn-on current of Q_3 in the lagging bridge under different the combinations shown in Figure 10a. The minimum current for ZVS performance can be inferred from (11).

$$i_b = \frac{(C_3 + C_4)V_{in}}{t_{dead}} = \frac{2 \times 120 \times 10^{-6} \times 400}{200 \times 10^{-9}} = 0.48A \tag{11}$$

where $C_3 = C_4 = 120$ pF, and $t_{dead} = 200$ ns.

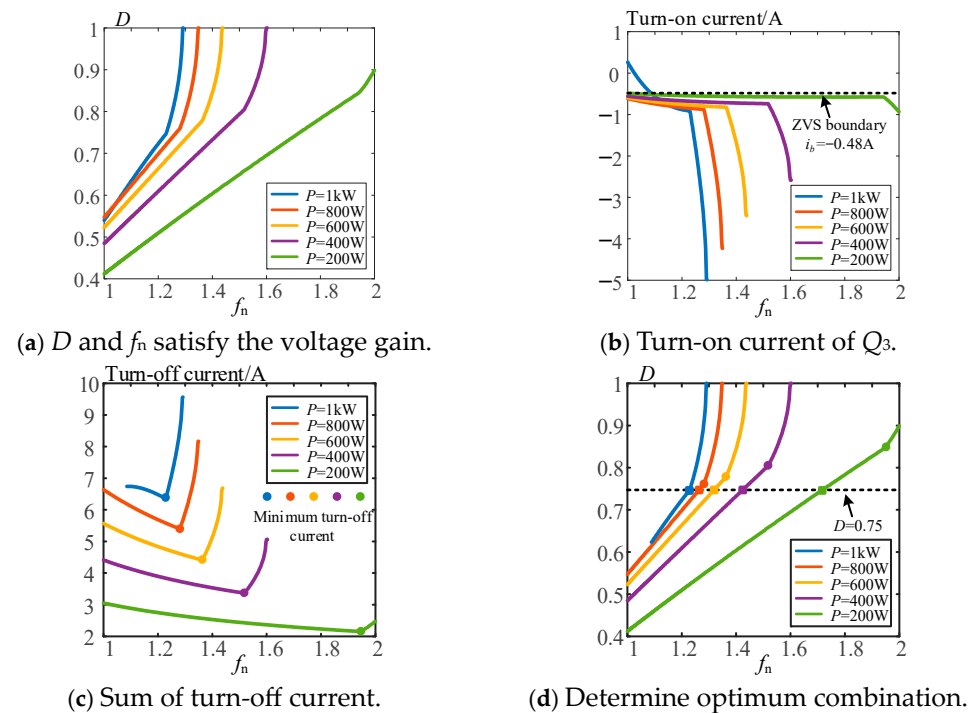


Figure 10. Hybrid control design for $V_{in} = 400$ V, and $V_o = 300$ V under different loads.

It can be seen that when the f_s is low and D is small, the turn-on current is not large enough to achieve ZVS, and the worst condition is that the polarity is opposite for the ZVS performance. To meet the ZVS constraint, the minimum value of duty cycle D needs to be constrained. Based on the ZVS constraint, the sum of the turn-off current of the leading-bridge and the lagging-bridge switches can be calculated. As Figure 10c shows, the operating point of the minimum-sum turn-off current is shown in a solid circle, and at that point the switching loss can be greatly reduced compared to the single PFM.

In the actual working condition, two control degrees will make the system complicated. For simplicity and reliability of the control, the combination of f_n and D can be treated as a constant D , which varies as the reference output voltage, and thus the constant D can be set as 0.75, as Figure 10d shows. The actual working point is close to the minimum turn-off current working point, which still maintains a small turn-off loss and leaves enough margin for the ZVS performance.

For simplicity and practicality, the adaptive duty cycle D can be summarized as a function of the reference output voltage based on the time-domain calculation results. Figure 11 is the fitted curve of the adaptive duty cycle D and reference V_o , and the fitted equation is shown in (12).

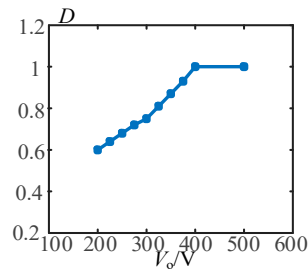


Figure 11. Fitted curve of adaptive duty cycle and reference V_o .

By presetting the duty cycle D according to the reference V_o , the two control degrees can be simplified to one degree, and no additional circuits need to be added.

$$D = \begin{cases} 0.002V_o + 0.1909 & V_o \in [200, 400] \\ 1 & V_o \in [400, 500] \end{cases} \quad (12)$$

4. Simulation Results

Based on the parameter shown in Table 3, simulation results are provided in this section. The proposed hybrid control method is compared to the single PFM or single PSM. The comparative data include the turn-on current of the lagging bridge, the sum of the turn-off current, peak resonant current and RMS resonant current, and the switching frequency f_s under full load and half load.

Figure 12 shows the V_{AB} and i_{Lr} waveforms when applying three control strategies under $V_o = 200$ V and $P = 1$ kW. For hybrid control, it can be seen that the ZVS performance is achieved; the turn-off current is 2.32A (lagging bridge) and 8.38A (leading bridge), and the sum is 10.7 A. For the single-PFM control method, although ZVS performance is achieved, the sum of the turn-off current is 16.54 A, which is 1.55 times that of 10.7 A. For single PSM, the ZVS performance of the lagging bridge is lost, due to a large phase-shifting angle. Table 4 presents all the comparative data: it can be seen the peak value and RMS value of i_{Lr} under hybrid control are almost same as the single PFM. Due to the reduced turn-off current and f_s , the turn-off loss is reduced by about 39.7%.

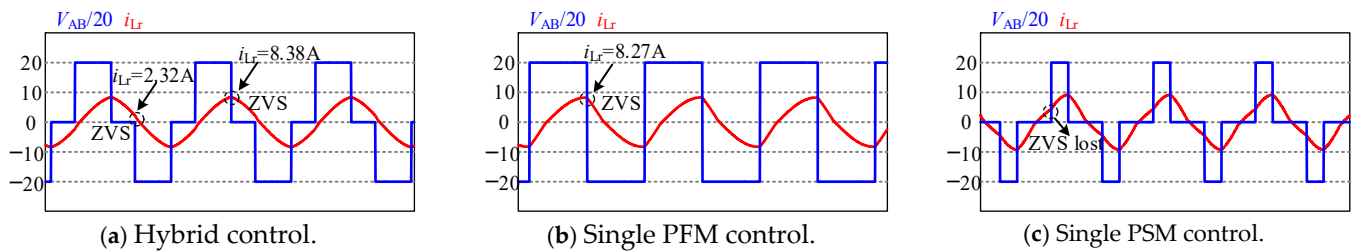


Figure 12. Simulation results under three control strategies @ $V_o = 200$ V $P = 1$ kW.

Table 4. Comparison of Different Control Strategies Under $V_o = 200$ V, $P = 1$ kW.

Parameter	Hybrid Control	Single PFM	Single PSM
D	0.6	1	0.33
ZVS	achieved	achieved	lost
Sum of turn-off current/A	10.70	16.54	\
i_{Lr} (peak)/A	8.43	8.30	\
i_{Lr} (rms)/A	5.61	5.65	5.81
f_s /kHz	177	190	142
Turn-off loss-reduction ratio	39.7%	Reference	\

Due to the limited space in this paper, the experiment results of other V_o and P values are concluded in Tables 5–7, while simulation waveforms are not provided. Table 5 shows

the simulation results under $V_o = 200\text{ V}$, $P = 500\text{ W}$; the conclusion is that when applying the hybrid control, ZVS performance is achieved, while it is lost under single PSM, and the sum turn-off current is 5.66 A. For single PFM, though ZVS performance is achieved, the sum of the turn-off current is 9.1 A, which is 1.62 times that of 5.66 A, and the peak value and RMS value of i_{Lr} in the hybrid control are almost the same as the single PFM. Due to the reduced turn-off current and f_s , the turn-off loss is reduced by about 44.7%.

Table 5. Comparison of Different Control Strategies Under $V_o = 200\text{ V}$, $P = 500\text{ W}$.

Parameter	Hybrid Control	Single PFM	Single PSM
D	0.6	1	0.33
ZVS	achieved	achieved	lost
Sum of turn-off current/A	5.66	9.1	\
i_{Lr} (peak)/A	4.46	4.58	\
i_{Lr} (rms)/A	2.84	2.88	3.27
f_s /kHz	213	240	142
Turn-off loss–reduction ratio	44.7%	Reference	\

Table 6. Comparison of Different Control Strategies Under $V_o = 300\text{ V}$, $P = 1\text{ kW}$.

Parameter	Hybrid Control	Single PFM	Single PSM
D	0.79	1	0.55
ZVS	achieved	achieved	lost
Sum of turn-off current/A	5.53	9.36	\
i_{Lr} (peak)/A	5.75	5.48	\
i_{Lr} (rms)/A	3.83	3.84	4.29
f_s /kHz	174	182	142
Turn-off loss–reduction ratio	43.5%	Reference	\

Table 7. Comparison of Two Control Strategies Under $V_o = 200\text{ V}$, $P = 1\text{ kW}$.

Parameter	Hybrid Control	Single PFM	Single PSM
D	0.67	1	0.43
ZVS	achieved	achieved	lost
Sum of turn-off current/A	12.80	17.6	\
i_{Lr} (peak)/A	8.6	8.8	\
i_{Lr} (rms)/A	5.66	5.80	5.60
f_s /kHz	182	190	142
Turn-off loss–reduction ratio	30.3%	Reference	\

Table 6 shows the simulation results under $V_o = 300\text{ V}$, $P = 1\text{ kW}$. Due to $V_o = 300$, the adaptive D changes to 0.79, according to (12). The conclusion is that when applying the hybrid control, ZVS performance is achieved, while it is lost under single PSM, and the sum of the turn-off current is 5.53 A. For single PFM, though ZVS performance is achieved, the sum of the turn-off current is 9.36 A, which is 1.69 times that of 5.53 A, and the peak value and RMS value of i_{Lr} in the hybrid control are almost the same as the single PFM. Due to the reduced turn-off current and f_s , the turn-off loss is reduced by about 43.5%.

5. Experiment Results

In this section, a 1-kW/ $V_o = 200\text{--}500\text{ V}$ experimental prototype is built to validate the theoretical analysis and feasibility of the hybrid control method. The experimental platform is shown in Figure 13, and the parameter of the converter is shown as Table 3. Three groups of experiments are developed including $V_o = 200\text{ V}$ ($P = 1\text{ kW}/500\text{ W}$), and $V_o = 300\text{ V}$ ($P = 1\text{ kW}$) under the hybrid control method, single PFM and single PSM. To ensure ZVS performance, the adaptive duty cycle D of the hybrid control maintains a margin of about 10% with respect to the theoretical-analysis results.



Figure 13. Experimental platform.

Figure 14 shows the waveforms of V_o , i_{Lr} and V_{AB} under $V_o = 200$ V and $P = 1$ kW, and the experiment results are concluded in Table 7. The adaptive D is 0.66 according to reference V_o , and it can be seen that ZVS performance can be obtained under hybrid control, while it is lost under the single-PSM control method. The sum of the turn-off current under hybrid control is 12.8 A, while it is 17.6 A under single PFM; the turn-off loss under hybrid control can reduce to about 30.3% of that of single PFM when taking f_s into consideration. The peak value and RMS value of i_{Lr} are 8.6A and 5.66A under hybrid control, while they are 8.8 A and 5.8 A under single PFM. The switching frequency f_s of the two control methods are 182 kHz and 190 kHz, which means the other power losses are almost the same for the two control methods.

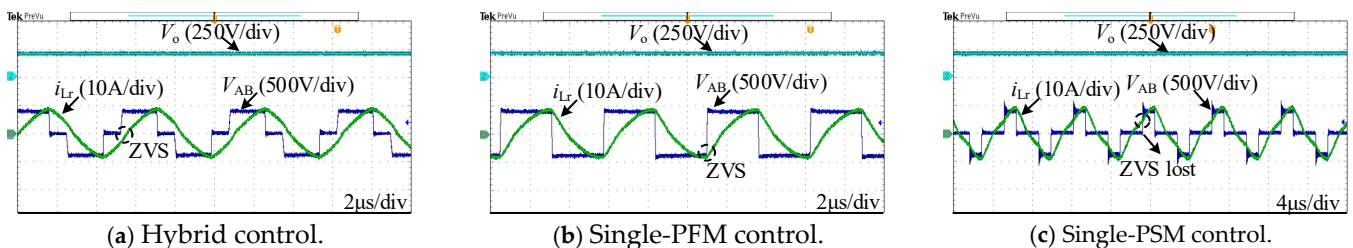


Figure 14. Experimental results under three control strategies @ $V_o = 200$ V $P = 1$ kW.

Figure 15 shows the waveforms of V_o , i_{Lr} and V_{AB} under $V_o = 200$ V and $P = 500$ W, and the experiment results are concluded in Table 8. The adaptive D is 0.66 according to V_o , and it can be seen that ZVS performance can be obtained under hybrid control, while it is lost under the single-PSM control method. The sum of the turn-off current under hybrid control is 7.2 A, while it is 9.2 A under single PFM; the turn-off loss under hybrid control can reduce by about 18.6%, compared to that of the single PFM when taking f_s into consideration. The peak value and RMS value of i_{Lr} are 4.6 A and 2.72 A under hybrid control, while they are 4.6 A and 2.92 A under single PFM. The switching frequency f_s of the two control methods are 226 kHz and 248 kHz, which means the other power losses are almost the same for the two control methods.

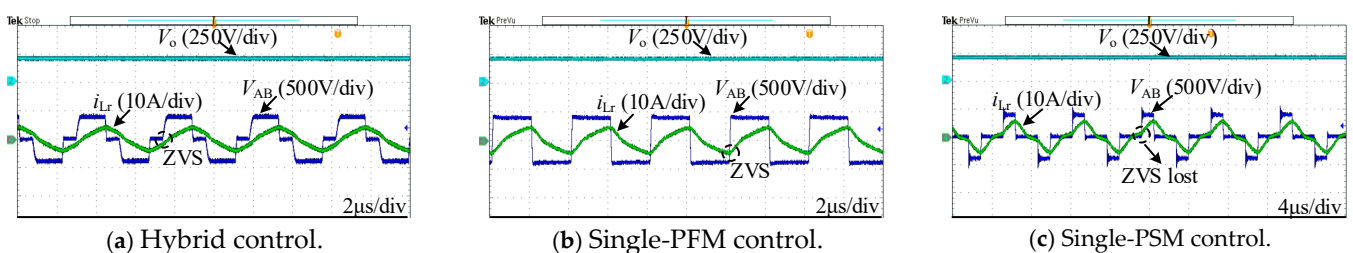
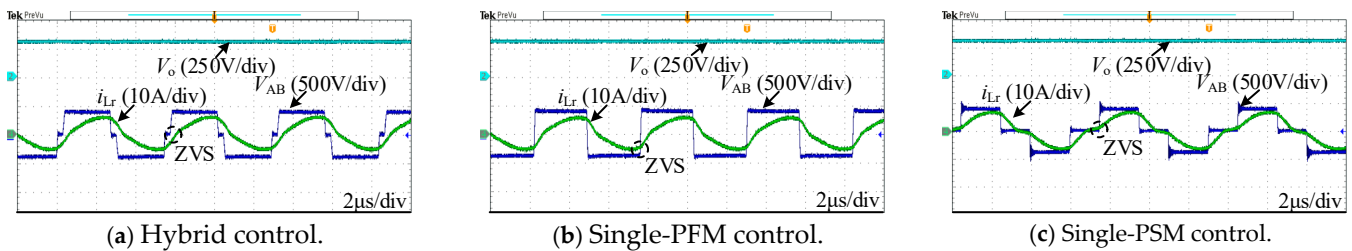


Figure 15. Experimental results under three control strategies @ $V_o = 200$ V $P = 500$ W.

Table 8. Comparison of Two Control Strategies Under $V_o = 200\text{ V}$, $P = 500\text{ W}$.

Parameter	Hybrid Control	Single PFM	Single PSM
D	0.67	1	0.42
ZVS	achieved	achieved	lost
Sum of turn-off current/A	7.2	9.2	\
i_{Lr} (peak)/A	4.6	4.6	\
i_{Lr} (rms)/A	2.72	2.92	3.17
f_s /kHz	226	248	142
Turn-off loss–reduction ratio	18.6%	Reference	\

Figure 16 shows the waveforms of V_o , i_{Lr} and V_{AB} under $V_o = 300\text{ V}$ and $P = 1\text{ kW}$, and the experiment results are concluded in Table 9. The adaptive D changes to 0.88; according to the reference V_o , it can be seen that ZVS performance can be obtained under hybrid control, while it is lost under single PSM. The sum of the turn-off current under hybrid control is 9.6 A, while it is 10.4 A under single PFM; the turn-off loss under hybrid control can reduce by about 8.7% compared to that of the single PFM when taking f_s into consideration. The peak value and RMS value of i_{Lr} are 5.8 A and 4 A under hybrid control, while they are 5.6 A and 3.96 A under single PFM; the switching frequency f_s of the two control methods are 183 kHz and 185 kHz, which means the other power losses are almost same for the two control methods. Owing to the adaptive D (0.88) being large, the hybrid control comes close to the single PFM, and thus the turn-off loss–reduction ratio is small. Therefore, the hybrid control method is more suitable for wide voltage-gain range application where the voltage gain reaches a low value.

**Figure 16.** Experimental results under three control strategies @ $V_o = 300\text{ V}$, $P = 1\text{ kW}$.**Table 9.** Comparison of Two Control Strategies Under $V_o = 300\text{ V}$, $P = 1\text{ kW}$.

Parameter	Hybrid Control	Single PFM	Single PSM
D	0.88	1	0.56
ZVS	achieved	achieved	lost
Sum of turn-off current/A	9.6	10.4	\
i_{Lr} (peak)/A	5.8	5.6	\
i_{Lr} (rms)/A	4	3.96	4.33
f_s /kHz	183	185	142
Turn-off loss–reduction ratio	8.7%	Reference	\

For the LLC resonant converter, its main loss comes from the turn-off loss and on-state loss. Through hybrid modulation, the switching frequency can be reduced and the turn-off current can be reduced. When the operation conditions are consistent, lower loss and higher efficiency can be achieved than with the single-modulation technique. To verify the effectiveness of hybrid control for reducing the power loss, the efficiency comparison is developed under hybrid control, single PFM and single PSM at $V_o = 200\text{ V}$ and 300 V . As Figure 17 shows, the efficiency of the hybrid control is higher than PFM and PSM. At $V_o = 200\text{ V}$, the efficiency improvement is between 0.75 and 1.4%, compared to the single PFM. At $V_o = 300\text{ V}$, due to the adaptive D being large, the operating characteristic of the hybrid control is nearly that of the single PFM, and the improvement of efficiency is

slight. For PSM, due to the loss of ZVS performance, the efficiency reduces to below 90%, at $V_o = 200$ V.

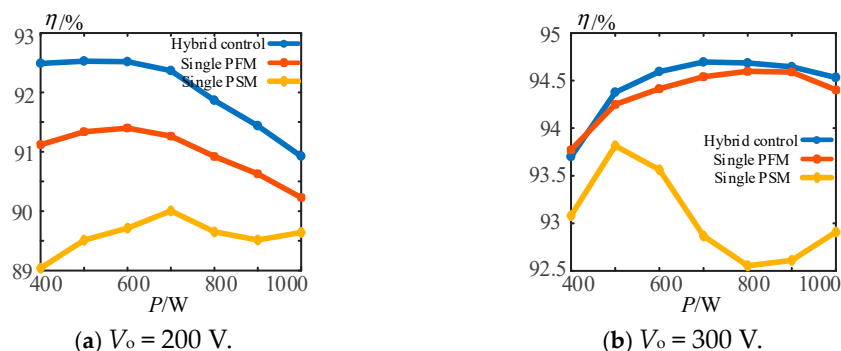


Figure 17. Efficiency comparison.

6. Conclusions

In this paper, a hybrid control method with adaptive PSM and PFM is proposed to maintain ZVS performance and reduce turn-off loss for the LLC resonant converter operating at wide voltage-gain range. Mode characteristics and soft-switching performance characteristics of different modes when applying PSM are illustrated. Based on time domain analysis, the turn-on current of the primary-side switches is calculated, and thus the ZVS boundary of different phase-shifting-angle- θ and switching-frequency- f_s combinations is inferred. In addition, to acquire the optimum steady-state operation of the converter, the turn-off current is calculated; by making the converter work near to the minimum turn-off current operating point, the turn-off loss can be greatly reduced. With the principles of the ZVS boundary and minimum turn-off current, the phase-shifting angle θ of PSM is designed to be adaptive to the reference output voltage, no additional circuits are needed, and the two control degrees (θ and f_s) are simplified to one (f_s). The simulation and a 1 kW/output voltage 200–500 V experimental prototype are built to validate the feasibility and effectiveness of the proposed hybrid control method. Both results show the hybrid control method can maintain ZVS performance at wide output voltage range and wide load range when compared to single PSM, and the sum of the turn-off currents of the primary-side leading- and lagging-bridge switches is reduced when compared to single PFM; thus, turn-off loss is reduced. The efficiency comparison validates the fact that the hybrid control method has less power loss than single PSM and single PFM. Through the proposed hybrid-modulation technology, efficiency can be improved, and for data centers and charging-pile power consumption sites, a small efficiency increase can bring huge benefits.

Author Contributions: Methodology, H.J.; Formal analysis, X.Y.; Data curation, H.J.; Writing—original draft, H.J.; Writing—review & editing, X.Y.; Funding acquisition, X.Y. All authors have read and agreed to the published version of the manuscript.

Funding: This research was funded by the National Natural Science Foundation Youth Project of China, grant number 52107195.

Data Availability Statement: Data are contained within the article.

Conflicts of Interest: The authors declare no conflicts of interest.

References

- Tran, Y.; Freijedo, F.D.; Dujic, D. Open-Loop Power Sharing of Three-Port DC-DC Resonant Converters. In Proceedings of the 2019 IEEE Applied Power Electronics Conference and Exposition (APEC), Anaheim, CA, USA, 17–21 March 2019; pp. 2138–2144.
- Deng, J.; Li, S.; Hu, S.; Mi, C.C.; Ma, R. Design Methodology of LLC Resonant Converters for Electric Vehicle Battery Chargers. *IEEE Trans. Veh. Technol.* **2014**, *63*, 1581–1592. [\[CrossRef\]](#)
- Chen, S.; Li, Z.R.; Chen, C. Analysis and Design of Single-Stage AC/DC LLC Resonant Converter. *IEEE Trans. Ind. Electron.* **2012**, *59*, 1538–1544. [\[CrossRef\]](#)

4. Wei, Y.; Luo, Q.; Wang, Z.; Mantooth, A.; Zhao, X. Comparison between Different Analysis Methodologies for LLC Resonant Converter. In Proceedings of the 2019 IEEE Energy Conversion Congress and Exposition (ECCE), Baltimore, MD, USA, 29 September–3 October 2019; pp. 4429–4434.
5. Cao, Q.; Li, Z.; Wang, H. Wide Voltage Gain Range LLC DC/DC Topologies: State-of-the-Art. In Proceedings of the 2018 International Power Electronics Conference (IPEC–Niigata 2018–ECCE Asia), Niigata, Japan, 20–24 May 2018; pp. 100–107.
6. Wei, Y.; Luo, Q.; Mantooth, A. Overview of Modulation Strategies for LLC Resonant Converter. *IEEE Trans. Power Electron.* **2020**, *35*, 10423–10443. [[CrossRef](#)]
7. Soeiro, T.B.; Mühlethaler, J.; Linnér, J.; Ranstad, P.; Kolar, J.W. Automated Design of a High-Power High-Frequency LCC Resonant Converter for Electrostatic Precipitators. *IEEE Trans. Ind. Electron.* **2013**, *60*, 4805–4819. [[CrossRef](#)]
8. Chen, Y.; Xu, J.; Gao, Y.; Lin, L.; Cao, J.; Ma, H. Analysis and Design of Phase-Shift Pulse-Frequency-Modulated Full-Bridge LCC Resonant Converter. *IEEE Trans. Ind. Electron.* **2020**, *67*, 1092–1102. [[CrossRef](#)]
9. Zhe, L.; Chun-Yoon, P.; Jung-Min, K.; Bong-Hwan, K. High-Power-Factor Single-Stage LCC Resonant Inverter for Liquid Crystal Display Backlight. *IEEE Trans. Ind. Electron.* **2011**, *58*, 1008–1015.
10. Bingham, C.M.; Ann, A.Y.; Foster, M.P.; Stone, D.A. Analysis and Control of Dual-Output LCLC Resonant Converters with Significant Leakage Inductance. *IEEE Trans. Power Electron.* **2008**, *23*, 1724–1732. [[CrossRef](#)]
11. Shafiei, N.; Pahlevaninezhad, M.; Farzanehfard, H.; Motahari, S.R. Analysis and Implementation of a Fixed-Frequency LCLC Resonant Converter with Capacitive Output Filter. *IEEE Trans. Ind. Electron.* **2011**, *58*, 4773–4782. [[CrossRef](#)]
12. Qu, X.; Wong, S.; Tse, C.K. An Improved LCLC Current-Source-Output Multistring LED Driver With Capacitive Current Balancing. *IEEE Trans. Power Electron.* **2015**, *30*, 5783–5791. [[CrossRef](#)]
13. Chen, Y.; Wang, H.; Hu, Z.; Liu, Y.; Afsharian, J.; Yang, Z.A. LCLC resonant converter for hold up mode operation. In Proceedings of the 2015 IEEE Energy Conversion Congress and Exposition (ECCE), Montreal, QC, Canada, 20–24 September 2015; pp. 556–562.
14. Kim, D.; Moon, S.; Yeon, C.; Moon, G. High-Efficiency LLC Resonant Converter with High Voltage Gain Using an Auxiliary LC Resonant Circuit. *IEEE Trans. Power Electron.* **2016**, *31*, 6901–6909. [[CrossRef](#)]
15. Jeong, Y.; Moon, G.; Kim, J. Analysis on half-bridge LLC resonant converter by using variable inductance for high efficiency and power density server power supply. In Proceedings of the 2017 IEEE Applied Power Electronics Conference and Exposition (APEC), Tampa, FL, USA, 26–30 March 2017; pp. 170–177.
16. Chung, S.K.; Kang, B.G.; Kim, M.S. Constant frequency control of LLC resonant converter using switched capacitor. *Electron. Lett.* **2013**, *49*, 1556–1557. [[CrossRef](#)]
17. Hu, Z.; Qiu, Y.; Wang, L.; Liu, Y. An Interleaved LLC Resonant Converter Operating at Constant Switching Frequency. *IEEE Trans. Power Electron.* **2014**, *29*, 2931–2943. [[CrossRef](#)]
18. Wu, X.; Bai, Z.; Ma, H. An LLC Converter Operating in Super-Wide Output Voltage Range with Variable-Mode Control Strategy. In Proceedings of the 2018 IEEE International Power Electronics and Application Conference and Exposition (PEAC), Shenzhen, China, 4–7 November 2018; pp. 1–6.
19. Li, Z.; Xue, B.; Wang, H. An Interleaved Secondary-Side Modulated LLC Resonant Converter for Wide Output Range Applications. *IEEE Trans. Ind. Electron.* **2020**, *67*, 1124–1135. [[CrossRef](#)]
20. Li, C.; Wang, H. A Wide Gain Range LLC Resonant Converter Based on Reconfigurable Bridge and Asymmetric Resonant Tanks. In Proceedings of the 2019 IEEE Applied Power Electronics Conference and Exposition (APEC), Anaheim, CA, USA, 17–21 March 2019; pp. 3281–3286.
21. Zhao, Q.; Zhang, J.; Gao, Y.; Wang, D.; Yang, Q. Hybrid Variable Frequency LLC Resonant Converter with Wide Output Voltage Range. *IEEE Trans. Power Electron.* **2023**, *38*, 11038–11049. [[CrossRef](#)]
22. Wang, L.; Wang, H.; Xue, B.; Zhou, M. H5-Bridge-Based Single-Input–Dual-Output LLC Converter with Wide Output Voltage Range. *IEEE Trans. Ind. Electron.* **2022**, *69*, 7008–7018. [[CrossRef](#)]
23. Wang, H.; Li, Z. A PWM LLC Type Resonant Converter Adapted to Wide Output Range in PEV Charging Applications. *IEEE Trans. Power Electron.* **2018**, *33*, 3791–3801. [[CrossRef](#)]
24. Jin, X.; Zhou, X.; Wang, W.; Ma, Z.; Xu, J.; Lu, Z. A Half-Bridge LLC Converter for Wide Input Voltage Range Applications. In Proceedings of the 2018 IEEE International Power Electronics and Application Conference and Exposition (PEAC), Shenzhen, China, 4–7 November 2018; pp. 1–5.
25. Liu, W.; Wang, B.; Yao, W.; Lu, Z.; Xu, X. Steady-state analysis of the phase shift modulated LLC resonant converter. In Proceedings of the 2016 IEEE Energy Conversion Congress and Exposition (ECCE), Milwaukee, WI, USA, 18–22 September 2016; pp. 1–5.
26. Kollipara, N.; Kazimierczuk, M.K.; Reatti, A.; Corti, F. Phase Control and Power Optimization of LLC Converter. In Proceedings of the 2019 IEEE International Symposium on Circuits and Systems (ISCAS), Sapporo, Japan, 26–29 May 2019; pp. 1–5.
27. Murata, K.; Kurokawa, F. Performance characteristic of interleaved LLC resonant converter with phase shift modulation. In Proceedings of the 2015 IEEE International Telecommunications Energy Conference (INTELEC), Osaka, Japan, 18–22 October 2015; pp. 1–5.
28. McDonald, B.; Wang, F. LLC performance enhancements with frequency and phase shift modulation control. In Proceedings of the 2014 IEEE Applied Power Electronics Conference and Exposition—APEC 2014, Fort Worth, TX, USA, 16–20 March 2014; pp. 2036–2040.
29. Kim, J.; Kim, C.; Kim, J.; Lee, J.; Moon, G. Analysis on Load-Adaptive Phase-Shift Control for High Efficiency Full-Bridge LLC Resonant Converter Under Light-Load Conditions. *IEEE Trans. Power Electron.* **2016**, *31*, 4942–4955.

30. Shakib, S.M.S.I.; Mekhilef, S. A Frequency Adaptive Phase Shift Modulation Control Based LLC Series Resonant Converter for Wide Input Voltage Applications. *IEEE Trans. Power Electron.* **2017**, *32*, 8360–8370. [[CrossRef](#)]
31. Kim, E.; Lee, J.; Heo, Y.; Marius, T. LLC resonant converter with wide output voltage control ranges operating at a constant switching frequency. In Proceedings of the 2018 IEEE Applied Power Electronics Conference and Exposition (APEC), San Antonio, TX, USA, 4–8 March 2018; pp. 2124–2128.
32. Sun, X.; Li, X.; Shen, Y.; Wang, B.; Guo, X. Dual-Bridge LLC Resonant Converter with Fixed-Frequency PWM Control for Wide Input Applications. *IEEE Trans. Power Electron.* **2017**, *32*, 69–80. [[CrossRef](#)]
33. Fei, C.; Li, Q.; Lee, F.C. Digital Implementation of Light-Load Efficiency Improvement for High-Frequency LLC Converters with Simplified Optimal Trajectory Control. *IEEE J. Emerg. Sel. Top. Power Electron.* **2018**, *6*, 1850–1859. [[CrossRef](#)]
34. Shi, L.; Liu, B.; Duan, S. Burst-Mode and Phase-Shift Hybrid Control Method of LLC Converters for Wide Output Range Applications. *IEEE Trans. Ind. Electron.* **2020**, *67*, 1013–1023. [[CrossRef](#)]
35. Fang, Z.; Huang, Z.; Jing, H.; Hu, G.; Wang, J.; Tao, L. A Novel Modulation Method of LLC Resonant Converter with Linear Model and High Efficiency. In Proceedings of the 2019 IEEE Energy Conversion Congress and Exposition (ECCE), Baltimore, MD, USA, 29 September–3 October 2019; pp. 5152–5155.

Disclaimer/Publisher’s Note: The statements, opinions and data contained in all publications are solely those of the individual author(s) and contributor(s) and not of MDPI and/or the editor(s). MDPI and/or the editor(s) disclaim responsibility for any injury to people or property resulting from any ideas, methods, instructions or products referred to in the content.